Available online at www.sciencedirect.com
ScienceDirect
Ceramics International 38 (2012) 663–670
CERAMICS INTERNATIONAL
www.elsevier.com/locate/ceramint

Characterization of alumina–alumina/graphite/monel superalloy brazed joints

S. Ghosh *, R. Chakraborty, N. Dandapat, K.S. Pal, S. Datta, D. Basu

Central Glass and Ceramic Research Institute, 196 Raja S.C. Mullick Road, Kolkata 700 032, India

Received 26 November 2010; received in revised form 1 May 2011; accepted 2 July 2011
Available online 30th July 2011

Abstract

Active metal brazing of alumina with alumina, graphite and monel 404 superalloy was performed at 910 °C for 5 min using TICUSIL (68.8Ag–26.7Cu–4.5Ti in wt.%) as the braze alloy in vacuum of 5×10^{-6} mbar. The brazed joints were characterized by X-ray diffraction, scanning electron microscopy, energy dispersive X-ray analysis, nanohardness and Young's modulus measurements by depth sensitive indentation technique. X-ray diffractrometry showed that the Ti-based compounds were formed at the substrate–filler alloy interfaces of the brazed joints as reaction products. The cross sectional microstructures of the brazed joints were observed by scanning electron microscopy. The energy dispersive X-ray analysis determined the elemental compositions at the selective points of the joint cross section, which supported the X-ray diffraction results. The nanohardness and Young's modulus of the substrate–filler alloy interface showed no abrupt change, which suggests reliable joint performance in service.

Keywords: A. Joining; B. X-ray methods; B. Microstructure-final; C. Hardness

1. Introduction

Advanced ceramics are becoming increasingly important in engineering applications because of their excellent strength, high thermal stability and high resistance to wear and corrosion. The inherent weakness of the material due to brittleness and poor machinability that restricts its fabrication only within simple geometries is being overcome by forming composites with metals or by joining them with metallic sub-systems [1]. Thus, there is an increasing demand to join ceramic-to-ceramic parts or ceramic components to metallic structures for structural applications. Therefore, suitable techniques are necessary for joining ceramic-to-ceramic or ceramic-to-metal components. Over the last few decades, researchers have adopted various methods to join ceramic to ceramic/metal parts such as diffusion bonding, brazing [2,3], solid-state bonding, liquid-state bonding, direct copper bonding [4], partial transient liquid phase bonding [5,6], a variant of the partial transient liquid phase method [7], solid-liquid interdiffusion and transient liquid phase techniques [8,9].

Most structural ceramics such as Al_2O_3, SiC, and ZrO_2 are chemically more stable than metals and cannot be wetted by traditional brazes unless the brazing alloy contains an active element [10]. Active metal brazing is a simple and economical method, which is utilized for joining ceramic-to-ceramic/metal components by using a filler metal wherein an active element (e.g. Ti, Zr, V, Cr) forms alloy with the base filler metal [10,11]. Titanium is most frequently used as an active element of silver-based active braze [10] that enhances wettability by reacting with the ceramic surface and changing its chemistry [11–13]. It has already been pointed out through several comprehensive reviews [14–19] that there are many critical factors (e.g. ceramic–metal combination, thermal expansion mismatch, ceramic surface condition, type and amount of the active element in the filler metal and brazing thermal cycle, etc.), which influence joining of ceramic to ceramic/metal components. Active brazing method has been successfully employed for joining of various ceramic–ceramic/metal parts [20–34].

Different brazed components of ceramics and metal/graphite are essential for development of several electron tubes such as magnetron, klystron, gyrotron, photomultiplier, X-ray tube,

* Corresponding author. Tel.: +91 033 2473 3469/76/77/96; fax: +91 033 2473 0957.
E-mail address: sumana@cgcri.res.in (S. Ghosh).

0272-8842/$36.00
doi:10.1016/j.ceramint.2011.07.054

traveling wave tube (TWT), cathode ray tube, etc. [35]. Recent revolution in communication technology has led to the increasing use of TWTs in some communications satellites as a good amplifier [36]. Consequently, development, characterization and reliability of such joints between dissimilar materials like alumina, high density graphite and monel alloy have become a subject of interest.

In the present work, alumina–alumina, alumina–graphite and alumina–monel 404 superalloy joining was conducted by active metal brazing technique with commercially available Ag–Cu–Ti filler metal and the joints were subsequently evaluated in terms of phase analysis of the substrate–filler alloy interfaces, microstructural examination and elemental composition analysis across the brazed joints. In addition, relative nanohardness and Young's modulus measurements of interfaces, substrates and filler alloy were performed to assess the suitability of the joints in actual service life.

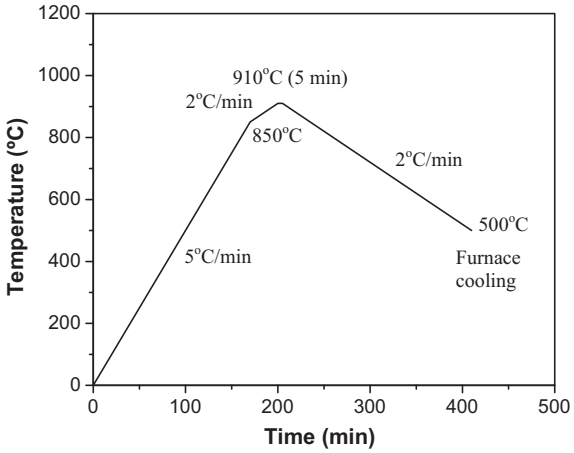

Fig. 1. Brazing temperature and time profile.

2. Experimental

Pure alumina powder (Alcoa, USA; 99.99% purity) was cold isostatically pressed to cylindrical shapes with 150 MPa pressure. The green powder compacts were dried, calcined in an electrical furnace (ELECTROHEAT, Model No. EN170QT, Naskar & Co., Howrah, India) at 800 °C for 1 h, cut into several pieces of specific size and finally sintered in an electrical furnace (ELECTROHEAT, Model No. EN170QT, Naskar & Co., Howrah, India) at 1600 °C for 2 h. The sintered alumina specimens had a dimension of 10 mm diameter and 2 mm thickness. The surfaces of sintered alumina specimens were ground in a grinding machine (Praga, India) with 6 μm diamond coated wheel and polished using 3 μm, 1 μm and 0.25 μm diamond paste. Discs of 10 mm diameter and 2 mm thickness were prepared from the other experimental materials, monel 404 superalloy (composition is given in Table 1) and poco graphite (high density graphite, 99.995% C). TICUSIL foil of 150 μm thickness with a composition of 68.8Ag–26.7Cu–4.5Ti in wt.% (WESGO, Inc., Hayward, CA 94544) was used as brazing alloy. The monel alloy samples were polished by SiC paper and subsequently by 1 and 0.25 μm alumina powder while the graphite samples were polished only with SiC paper of fine grit size. Prior to brazing, all the specimens were ultrasonically cleaned with acetone for 30 min. By keeping the filler alloy in between the alumina and other substrates, the sample assemblies were put inside a high vacuum furnace (Hindhivac Private Limited, Bangalore, India) where brazing was carried out at a temperature of 910 °C for 5 min with a vacuum of 5×10^{-6} mbar. The brazing thermal cycle is represented in Fig. 1.

Phase identification of the interfacial reaction products was carried out by X-ray diffractrometry (PW 1710, Philips Research Laboratory, Eindhoven, the Netherlands). For that purpose, one substrate of the brazed joint was first cut using a diamond wafering blade (Isomet, Buchler, USA) and thereafter the filler alloy was removed by grinding carefully. The brazed samples were cut along the cross-section by diamond wafering blade. The cut samples were then polished by a polishing machine (Buehler, USA) using 12 μm, 6 μm, 3 μm and 0.25 μm diamond paste and coated with thin gold layer for microstructural investigation by scanning electron microscopy (LEO S430i, LEO, UK). Elemental composition analysis was performed on the cross-sectional regions of the brazed joints by energy dispersive X-ray analysis technique (LEO S430i, LEO, UK, SiLi detector). The thermal expansion coefficient values of alumina, poco graphite and monel 404 superalloy were measured by a dilatometer (model-DIL 402C, Netzsch, Germany). Nanohardness and Young's modulus were measured across the brazed joints by Fischerscope (H100C XY_p, Fischer, Switzerland) using depth sensitive indentation technique [37,38]. A Berkovich indenter of 150 nm tip radius was used as the indenter. The force and depth sensing resolutions were 0.2 μN and 0.1 nm, respectively. The experiments were carried out at a load of 100 mN with 30 s loading/unloading time. A line array of 10 indentations was made for each region. The machine was calibrated by following the DIN 50359-1 standard with nanoindentation based independent evaluation of nanohardness (about 4.14 GPa) of a reference glass block (BK7, Schott, Germany) before each experiment.

Table 1
Composition of monel 404 super alloy.

C	Ni	Al	Fe	Mn	Si	S	Cu (in wt.%)
0.15	52–57	0.05	0.5	0.1	0.1	0.024	Balance

3. Results and discussion

An ideal joint should have compatibility with the working temperature, mechanical loading and environment in order to obtain prolonged life span [39]. The thermal residual stress generation due to mismatches in elastic modulus and thermal expansion coefficient of the base materials should be minimized, which enhances both the mechanical strength and reliability of the joint. The thermal expansion coefficients values of alumina, poco graphite and monel 404 superalloy were measured to be 8.1×10^{-6}/°C, 2.6×10^{-6}/°C and

13.5×10^{-6}/°C, respectively. The joining process and joint geometry should be optimized to avoid local stress concentration and maximize the joint strength. The composition and microstructure of the interface should be properly controlled to get high interfacial strength of the joint. The composition, thickness and morphology of interfacial reaction layers influence the joint strength. The joining defects at the interfacial regions and the residual stresses should be reduced to decrease the probability of crack nucleation and growth [39].

3.1. X-ray diffraction analysis

Fig. 2 shows the results of the X-ray diffraction (XRD) analysis of the interface regions of the brazed joints. In all the cases, the filler alloy diffused to the substrate surfaces, Ti element of the filler alloy reacted chemically with the joining surfaces and formed certain reaction products resulting in a strong chemical bond between the joint components. At the interface with alumina, Ti of brazing alloy was found to react with Al_2O_3 and produced TiO_2 and Ti_2O_3 (Fig. 2(a)) whereas reaction of Ti with graphite resulted in ε-$Ti_2C_{0.06}$ formation at the interface with graphite (Fig. 2(b)). On the other hand, during brazing, Ti reacted with monel alloy and formed several intermetallic compounds such as NiTi, Cu_3Ti, CuTi, $CuTi_3$, Cu_2Ti and Cu_4Ti_3 (Fig. 2(c)).

It has been reported that Ti from Cu–Ag–Ti based active brazing alloys reacts with alumina and forms a thin layer of oxides (e.g. TiO, Ti_2O_3, Ti_3O_5, Ti_4O_7 or TiO_2) whose stoichiometry depends on the activity of Ti in the filler alloy [39–41]. When alumina is brazed to different solids using reactive brazes the interaction between Ti and the elements contained in the solid can change the activity of Ti thus modifying both the thickness and the composition of the compound formed at the alumina/braze interface [42]. A second layer of reaction products can be formed on the primary oxide layer due to reaction of Ti with Cu from the filler alloy, which leads to mixed Ti–Cu oxides [43]. Suenaga et al. [43] and Barbier et al. [44] reported the presence of TiO, Ti_2O and Ti_3O_2 at the Ti containing filler alloy–alumina interface. Some researchers established that both Ti_4Cu_2O and Ti_3Cu_3O intermetallics can be formed in the reaction layer of alumina after brazing with Ti containing active filler alloys [44,45]. It is well established that the reaction between TICUSIL and alumina (homogeneous case) leads to the formation of M_6O-type $Ti_3(Cu,Al)_3O$ or $Ti_4(Cu,Al)_2O$ compounds responsible for the good wetting and the high adhesion [12]. The present XRD result of alumina–filler alloy interface region is in good agreement with the reported works [39–41]. However, in our case, absence of $Ti_4Cu_2O/Ti_4(Cu,Al)_2O$ and $Ti_3Cu_3O/Ti_3(Cu,Al)_3O$ intermetallic phases may be ascribed to the removal of second reaction layer by grinding of filler alloy. The formation of TiC in Ti-containing brazes in contact with carbon is thermodynamically favourable. Sub-stoichiometric carbides such as $TiC_{0.95}$, $TiC_{0.91}$, $TiC_{0.80}$, $TiC_{0.70}$, $TiC_{0.60}$ and $TiC_{0.48}$ can form by using the brazes having an activity of Ti greater than 0.1 [46,47]. The XRD result of graphite–filler alloy interface was matched with the earlier observations [27,46,47].

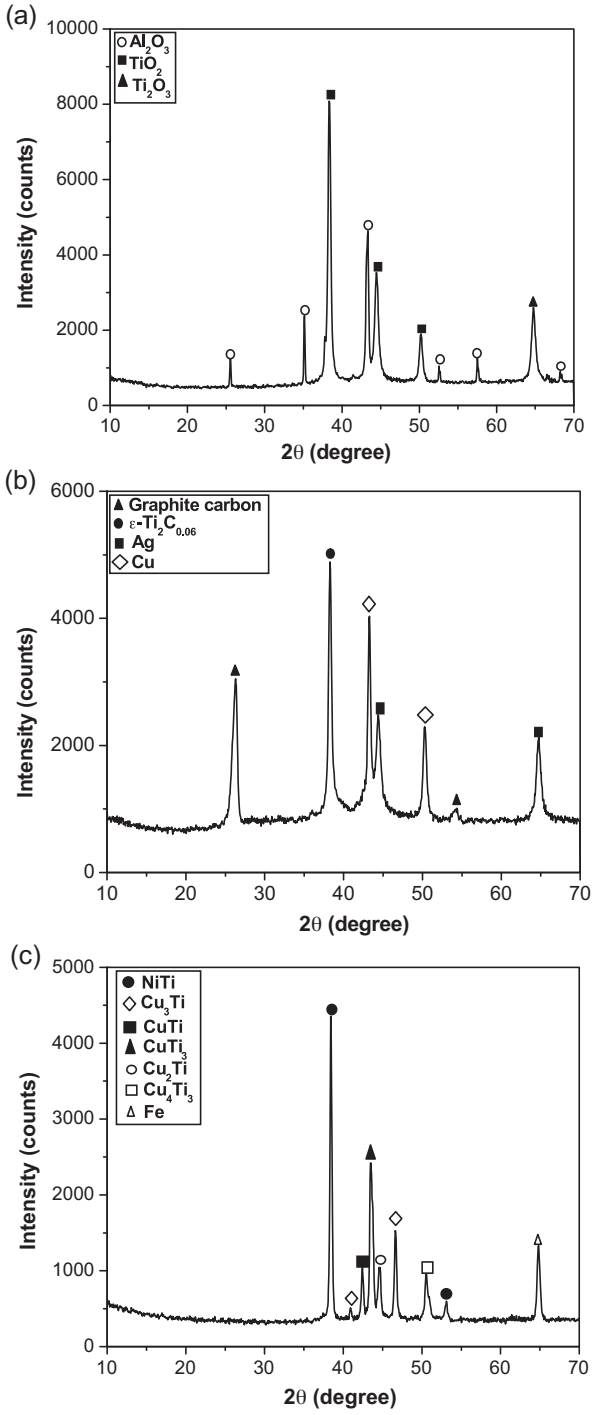

Fig. 2. XRD analysis of (a) alumina–braze interface of alumina–alumina joint, (b) graphite–braze interface of alumina–graphite joint and (c) monel alloy–braze interface of alumina–monel superalloy joint.

Shiue et al. found that Fe and Ni atoms of alloy 42 reacted with braze and consequently the reaction layer formed [10]. Similarly, in the present study, Ni and Cu elements of monel 404 alloy reacted with Ti of the brazing alloy and formed certain intermetallic compounds at the monel alloy–filler alloy interface. Thus, the XRD analysis clearly showed that in all the cases, the brazing alloy reacted chemically with the joining surfaces, which is a primary criterion of strong and reliable joint

formation. In the case of alumina–graphite and alumina–monel superalloy joints, the interactions between Ti and Ni and between Ti and carbon were very strong thus reducing strongly the activity of Ti [42].

3.2. Scanning electron microscopy (SEM) and energy dispersive X-ray (EDX) analysis

Fig. 3 shows the SEM microstructures of alumina, graphite and monel alloy substrates. The scanning electron micrographs and EDX analysis at the cross-sectional regions of brazed joints have been shown in Figs. 4–6. All the brazed interfaces were free from any crack or defect. Alumina and graphite had some open porosity leading to infiltration. For that reason, the thickness of the joints (Figs. 4 and 5) was four to five times lower than the thickness of TICUSIL foil. From Fig. 4(a and b), it can be observed that the reaction layer thickness was about 7 μm at the alumina–filler alloy interface while it was about 4 μm at the interface of graphite and filler alloy (Fig. 5(a and b)). On the contrary, the reaction layer was highly diffused in the monel–filler alloy interface, Fig. 6(a and b).

The results of EDX analysis along the cross-section of the alumina–alumina brazed joint at the regions marked as A–F of Fig. 4(b) are given in Fig. 4(c). Presence of Al, O, Ag elements was detected at 'A' and 'E' marked regions within alumina while Ag, Cu, Ti, Al and O elements were detected in 'B' and 'D' marked zones. Elements in 'C' marked regions mainly consisted of Ag, Cu, Ti and O. The EDX analysis across the alumina–alumina joint indicated that Ag, Cu and Ti elements diffused from brazing alloy to both alumina substrates, indicating a strong bonding. However, Ag diffused to the much inner side of both substrates. Presence of titanium and

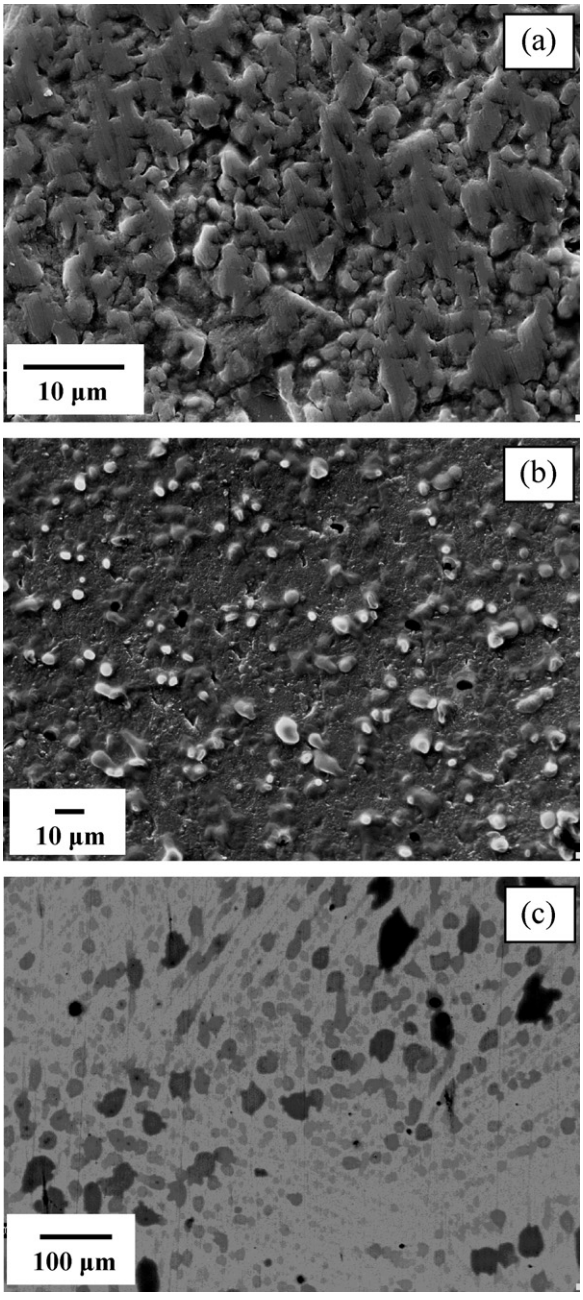

Fig. 3. Microstructures of (a) alumina ceramics, (b) graphite and (c) monel superalloy.

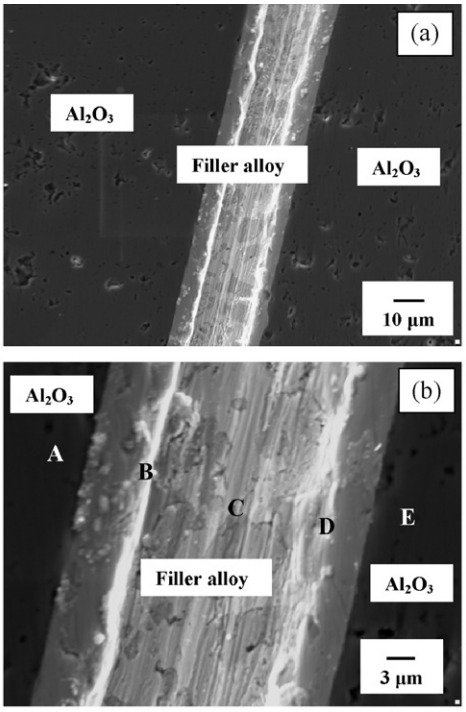

(c)

	Ag	Cu	Ti	Al	O
					(in atomic %)
A	0.49	-	-	37.09	62.42
B	0.51	32.02	39.85	6.37	21.25
C	11.10	4.26	55.73	-	28.91
D	4.53	3.78	58.77	8.57	24.35
E	0.55	-	-	41.73	57.72

Fig. 4. SEM and EDS analysis of the alumina–alumina brazed joint (a) cross-sectional view, (b) higher magnification of part (a) and (c) EDS analysis of A–E marked regions in part (b).

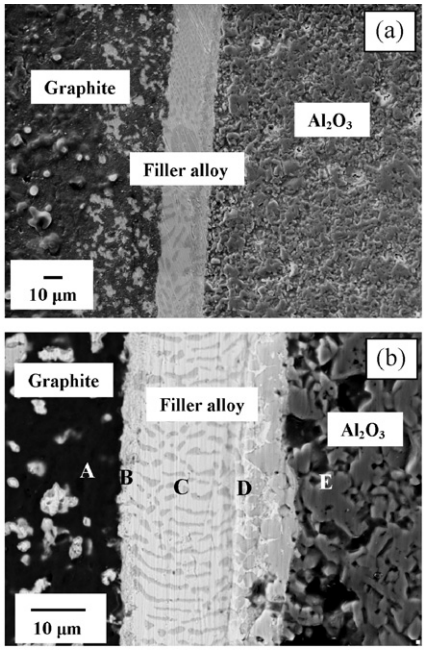

(c)

	Ag	Cu	Ti	C	Al	O
						(in atomic %)
A	0.18	-	0.86	88.27	-	10.69
B	2.73	33.31	31.62	26.99	0.85	4.50
C	26.37	11.50	24.32	20.81	0.44	16.56
D	5.45	3.84	12.54	19.16	14.65	44.36
E	-	-	-	18.43	25.68	55.89

Fig. 5. SEM and EDS analysis of the alumina–graphite brazed joint (a) cross-sectional view, (b) higher magnification of part (a) and (c) EDS analysis of A–E marked regions in part (b).

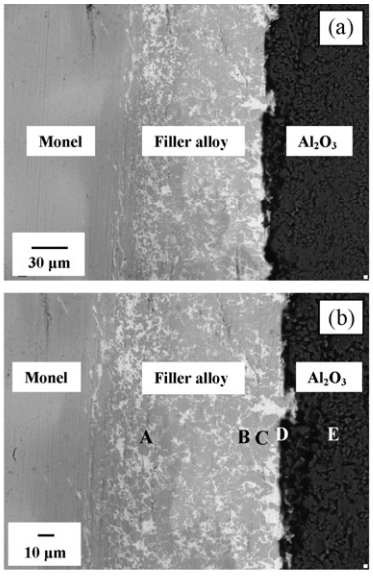

(c)

	Ag	Cu	Ti	Ni	Fe	Al	O
							(in atomic %)
A	0.57	20.57	3.84	64.09	1.03	1.74	8.16
B	31.07	5.65	7.42	23.69	0.36	1.50	30.31
C	37.45	20.87	9.31	17.23	-	1.39	13.75
D	1.71	0.91	4.51	14.63	-	22.82	55.42
E	0.51	-	-	-	-	50.14	49.35

Fig. 6. SEM and EDS analysis of the alumina–monel alloy brazed joint (a) cross-sectional view, (b) higher magnification of part (a) and (c) EDS analysis of A–E marked regions in part (b).

oxygen elements at the interfacial regions supported the XRD result (Fig. 2(a)). However, EDX analysis of point B (Fig. 4(c)) indicated the presence of M_6O-type $Ti_3(Cu,Al)_3O$ or $Ti_4(Cu,Al)_2O$ compounds at the alumina–braze interface as the ratio (Cu + Al)/Ti was very close to unity and the content in oxygen was higher than but very close to the theoretical value for M_6O [12].

EDX analysis (Fig. 5(c)) of the alumina–graphite joint at A–E regions of Fig. 5(b) showed that region 'A' contained Ag, Ti, C and O elements while Ag, Cu, Ti, C, Al and O elements were detected in the 'B', 'C' and 'D' marked regions. Regions marked as 'E' had C, Al and O elements. EDX analysis across the alumina–graphite joint showed that carbon diffused even into the alumina substrate through the filler alloy during brazing. Further, Ag, Ti and O elements diffused to the bulk side of the graphite component. The EDX data of the alumina–graphite joint at the interfaces supported the XRD result (Fig. 2(b)).

EDX analysis (Fig. 6(c)) of the alumina–monel alloy joint conducted at A–E regions of Fig. 6(b) showed the presence of Ag, Cu, Ti, Ni, Fe, Al and O elements in the 'A' and 'B' marked regions whereas 'C' and 'D' marked regions contained Ag, Cu, Ti, Ni, Al and O elements. Region 'E' was consisted of Ag, Al and O elements. EDX analysis confirmed the XRD results by detecting Ti and O elements at the alumina–filler alloy interface as well as Ti, Ni and Cu elements at the monel alloy–filler alloy interface. M_6O-type compounds were not formed at the graphite–braze and monel alloy–braze interfaces due to very strong Ti–Ni and Ti–C interactions [12]. In addition, the analysis showed that Ag element of brazing alloy diffused to both substrates while Cu and Ti elements diffused to monel side only from the braze. Al and O elements from alumina substrate diffused up to monel alloy part. It was assumed that monel alloy–braze interface was not clearly observed because of intensive interdiffusion of the elements between monel alloy and the braze material.

3.3. Nanohardness

When load is applied on the joint, soft filler metal accommodates the stress through plastic deformation [48]. However, at the substrate–filler alloy interfaces the deformation is restricted and as a result, local stress is concentrated at the interfacial regions [39]. Nanohardness distribution across the brazed joint indicates the extent of hardness differences between the filler alloy and the interfaces on either side. The large amount of hardness difference results in stress concentration at or near the interface on loading leading to

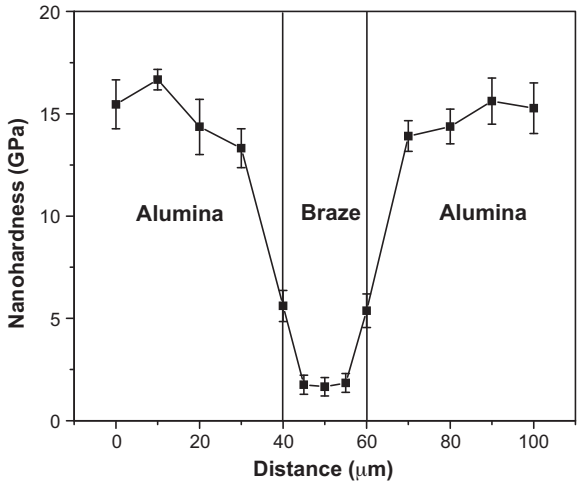

Fig. 7. Nanohardness profile across alumina–alumina brazed joint.

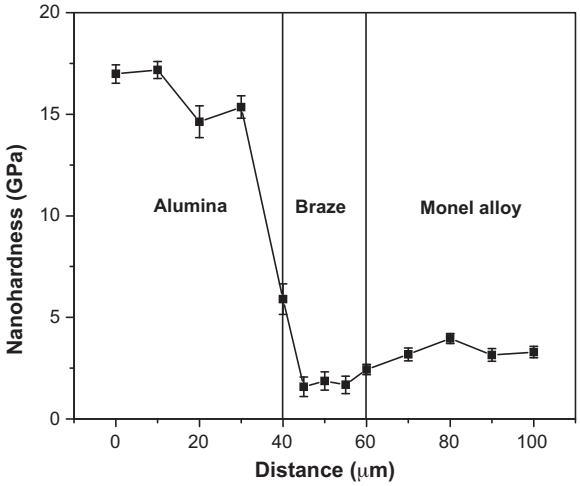

Fig. 9. Nanohardness profile across alumina–monel alloy brazed joint.

crack formation. Figs. 7–9 show the nanohardness distribution across the alumina–alumina and alumina–graphite and alumina–monel alloy joints. The nanohardness of alumina was about 15.25 ± 2.69 GPa, which reduced at the interface to about 5.71 ± 1.12 GPa and thereafter further to about 1.76 ± 0.58 GPa within the filler alloy (Fig. 7). The nanohardness values of graphite and graphite–braze interface were about 0.51 ± 0.08 GPa and 0.86 ± 0.5 GPa, respectively (Fig. 8). Similarly, the nanohardness of monel alloy was about 3.49 ± 0.72 GPa whereas in the monel–braze interface it was about 2.44 ± 0.25 GPa. The results showed that the nanohardness of braze was lower than those of alumina and monel alloy (Fig. 9). However, graphite had lower nanohardness than that of braze. The nanohardness value of interfacial region between the joined part and braze was intermediate with respect to their individual nanohardness values, which may be due to the formation of many new phases. However, the gradual and systematic changes of hardness across the interfaces indicate that no brittle phase of high hardness was formed at the braze-substrate interfaces, which in turn establishes the reliability of the joints.

3.4. Young's modulus

The Young's modulus measurements across the brazed joint provide information about the stiffness differences between the substrate–filler alloy interfaces and the filler alloy. Under stress, cracks are formed at the interfaces of the brazed joints due to steep stiffness differences between the interfaces and the filler alloy [39]. The Young's modulus values of alumina, alumina–braze interface and braze across the alumina–alumina joint have been given in Table 2. The results showed that the Young's modulus value reduced progressively from the alumina to the filler alloy. Table 3 shows the Young's modulus values of alumina, alumina–braze interface, braze, graphite–braze interface and graphite along the cross-section of the alumina–graphite joint. The graphite showed lowest Young's modulus in this system. The Young's modulus of graphite–braze interface

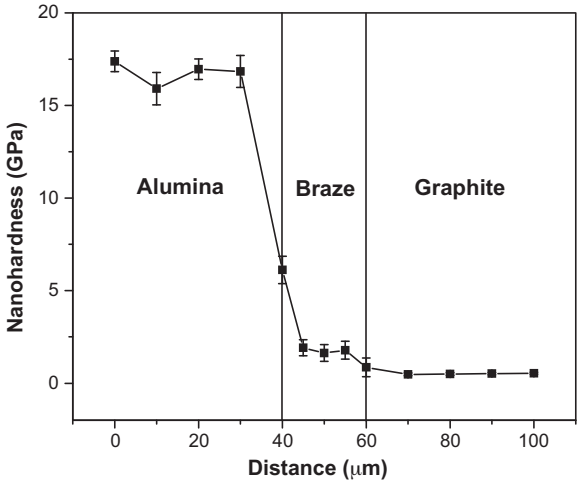

Fig. 8. Nanohardness profile across alumina–graphite brazed joint.

Table 2
Young's modulus data across alumina–alumina joint.

Young's modulus data	(in GPa)
Alumina	397.72 ± 46.43
Alumina–braze layer interface	347.26 ± 35.84
Braze layer	221.19 ± 18.63

Table 3
Young's modulus data across alumina–graphite joint.

Young's modulus data	(in GPa)
Alumina	395.84 ± 49.76
Alumina–braze layer interface	351.67 ± 33.85
Braze layer	198.33 ± 21.23
Graphite–braze layer interface	39.77 ± 6.40
Graphite	28.29 ± 8.33

Table 4
Young's modulus data across alumina–monel alloy joint.

Young's modulus data	(in GPa)
Alumina	393.66 ± 56.80
Alumina–braze layer interface	355.18 ± 32.46
Braze layer	192.74 ± 19.56
Monel–braze layer interface	204.32 ± 14.12
Monel	293.35 ± 34.24

was higher compared to that of graphite but lower than that of braze. In alumina–monel joint (Table 4) as the monel alloy had higher Young's modulus than those of monel–braze interface and braze alloy, the values across the joint decreased gradually from alumina to braze and thereafter slowly increased again in the monel side. All the above data did not show any abrupt changes near the interfaces, which indicates that the joints would be quite reliable during load application.

4. Conclusions

Alumina was joined with alumina, graphite and monel superalloy by active metal brazing technique. X-ray diffractometry and energy dispersive X-ray analysis identified thin Ti-based compounds as reaction products at all the interfaces of the brazed joints confirming good bond strength. Microstructural examination by scanning electron microscopy showed that the interfacial regions were devoid of any crack or defect. The nanohardness and Young's modulus measurements showed excellent transition between the substrate materials of the brazed joint, indicating reliable joint performance during service.

Acknowledgements

The authors are very grateful to Prof. I. Manna, Director, Central Glass and Ceramic Research Institute, Kolkata 700 032, India, for his kind permission to publish this paper. The authors are thankful to Dr. S. Majumder, Mr. A. K. Mandal and Mr. A. Dey for their assistance in doing XRD, SEM, EDX, nanohardness and Young's modulus measurements, respectively.

References

[1] H.Q. Hao, Y.L. Wang, Z.H. Jin, X.T. Wang, Joining of zirconia to zirconia using Ag–Cu–Ti filler metal, J. Mater. Process. Technol. 52 (1995) 238–247.
[2] T. Wagner, R. Kirchheim, M. Rühle, Chemical reactions at metal/ceramic interfaces during diffusion bonding, Acta. Metall. Mater. 43 (1995) 1053–1063.
[3] A.-P. Xian, Z.-Y. Si, Joining of Si_3N_4 using $Ag_{57}Cu_{38}Ti_5$ brazing filler metal, J. Mater. Sci. 25 (1990) 4483–4487.
[4] A. Kara-Slimane, D. Juve, E. Leblond, D. Treheux, Joining of AlN with metals and alloys, J. Eur. Ceram. Soc. 20 (2000) 1829–1836.
[5] Y. Iino, Partial transient liquid-phase metals layer technique of ceramic–metal bonding, J. Mater. Sci. Lett. 10 (1991) 104–106.
[6] M.L. Salz, B.J. Dalgleish, A.P. Tomsia, A.M. Glaeser, Ceramic joining, J. Mater. Sci. 28 (1993) 1673–1684.
[7] R.A. Marks, J.D. Sugar, A.M. Glaeser, Ceramic joining IV. effects of processing conditions on the properties of alumina joined via Cu/Nb/Cu interlayers, J. Mater. Sci. 36 (2001) 5609–5624.
[8] L. Bernstein, H. Bartholomew, Application of solid liquid interdiffusion (SLID) bonding in integrated circuit fabrication, Trans. AIME 236 (1966) 405–412.
[9] D.S. Duvall, W.A. Owczarski, D.F. Paulonis, TLP bonding: a new method for joining heat resistant alloys, Weld. J. 53 (1974) 203–214.
[10] R.K. Shiue, S.K. Wu, O. J.M., J.Y. Wang, Microstructural evolution at the bonding interface during the early-stage infrared active brazing of alumina, Metall. Mater. Trans. A 31A (2000) 2527–2536.
[11] A. Kar, S. Mandal, K. Venkateswarlu, A.K. Ray, Characterization of interface of Al_2O_3–304 stainless steel braze joint, Mater. Charact. 58 (2007) 555–562.
[12] R. Voytovych, F. Robaut, N. Eustathopoulos, The relation between wetting and interfacial chemistry in the CuAgTi/alumina system, Acta Mater. 54 (2006) 2205–2214.
[13] R.E. Loehman, A.P. Tomsia, Acta Mater. 40 (1994) 547.
[14] H. Mizuhara, K. Mally, Ceramic-to-metal joining with active brazing filler metal, Weld. J. 64 (1985) 27–32.
[15] H. Mizuhara, E. Huebel, Joining ceramic to metal with ductile active filler metal, Weld. J. 65 (1985) 43–51.
[16] A.H. Carim, R.E. Leohman, Microstructure at the interface between AIN and a Ag–Cu–Ti braze alloya), J. Mater. Res. 5 (1990) 1520–1529.
[17] M.G. Nicholas, D.A. Mortimer, Ceramic/metal joining for structural applications, Mater. Sci. Technol. 1 (1985) 657–665.
[18] R.E. Loehman, A.P. Tomsia, Joining of ceramics, Am. Ceram. Soc. Bull. 67 (1988) 375–380.
[19] H. Mizuhara, E. Huebel, T. Oyama, High-reliability joining of ceramic to metal, Am. Ceram. Soc. Bull. 67 (1988) 1591–1599.
[20] Y.H. Chai, W.P. Weng, T.H. Chuang, Relationship between wettability and interfacial reaction for Sn10Ag4Ti on Al_2O_3 and SiC substrates, Ceram. Int. 24 (1998) 273–279.
[21] S.H. Yang, S. Kang, Fracture behavior and reliability of brazed alumina joints via Mo–Mn process and active metal brazing, J. Mater. Res. 15 (2000) 2238–2243.
[22] D. Travessa, M. Ferrante, G–d. Ouden, Diffusion bonding of aluminium oxide to stainless steel using stress relief interlayers, Mater. Sci. Eng. A 337 (2002) 287–296.
[23] H. Ning, Z. Geng, J. Ma, F. Huang, Z. Qian, Z. Han, Joining of sapphire and hot pressed Al_2O_3 using $Ag_{70.5}$ $Cu_{27.5}$ Ti_2 brazing filler metal, Ceram. Int. 29 (2003) 689–694.
[24] I. Chakravarty, S.P. Gupta, Formation of intermetallics during brazing of alumina with Fe, Ni and Cr using Ag–30 Cu–10 Sn as filler metal, Mater. Charact. 51 (2003) 235–241.
[25] G.J. Qiao, C.G. Zhang, Z.H. Jin, Thermal cyclic test of alumina/kovar joint brazed by Ni–Ti active filler, Ceram. Int. 29 (2003) 7–11.
[26] S. Mandal, A.K. Ray, A.K. Ray, Correlation between the mechanical properties and the microstructural behaviour of Al_2O_3–(Ag–Cu–Ti) brazed joints, Mater. Sci. Eng. A 383 (2004) 235–244.
[27] P. Prakash, T. Mohandas, P. Dharma Raju, Microstructural characterization of SiC ceramic and SiC–metal active metal brazed joints, Scr. Mater. 52 (2005) 1169–1173.
[28] A. Kar, S.P. Sagar, A.K. Ray, Characterization of the ceramic–metal brazed interface using ultrasonic technique, Mater. Lett. 61 (2007) 4169–4172.
[29] M. Nomura, C. Iwamoto, S.I. Tanaka, Nanostructure of wetting triple line in a Ag–Cu–Ti/Si_3N_4 reactive system, Acta Mater. 47 (1999) 407–413.
[30] R.E. Loehman, A.P. Tomsia, Reactions of Ti and Zr with AlN and Al_2O_3, Acta. Metall. Mater. 40 (1992) S75–S83.
[31] R.E. Loehman, A.P. Tomsia, Wetting and joining of mullite ceramics by active-metal braze alloys, J. Am. Ceram. Soc. 77 (1994) 271–274.
[32] R. Asthana, M. Singh, Joining of partially sintered alumina to alumina, titanium, hastealloy and C–SiC composite using Ag–Cu brazes, J. Eur. Ceram. Soc. 28 (2008) 617–631.
[33] O. Kozlova, M. Braccini, R. Voytovych, N. Eustathopoulos, P. Martinetti, M.-F. Devismes, Brazing copper to alumina using reactive CuAgTi alloys, Acta Mater. 58 (2010) 1252–1260.
[34] O.C. Paiva, M.A. Barbosa, Microstructure, mechanical properties and chemical degradation of brazed AISI 316 stainless steel/alumina systems, Mater. Sci. Eng. A 480 (2008) 306–315.

[35] K. Henney, J.D. Fahnestock, Electron Tubes in Industry, third ed., London, 1952
[36] K. Yamamoto, Y. Morishita, M. Sasaki, Research and development of traveling wave tubes for broadcasting satellites, Space Jpn. Rev. 2–3 (2006) 1–10.
[37] N.K. Mukhopadhyay, P. Paufler, Micro- and nanoindentation techniques for mechanical characterisation of materials, Int. Mater. Rev. 51 (2006) 209–245 (37).
[38] W.C. Oliver, G.M. Pharr, An improved technique for determining hardness and elastic modulus using load and displacement sensing indentation experiments, J. Mater. Res. 7 (1992) 1564–1583.
[39] R.M. do Nascimento, A.E. Martinelli, A.J.A. Buschinelli, Review article: recent advances in metal–ceramic brazing, Cerâmica 49 (2003) 178–198.
[40] J.J. Pak, M.L. Santella, R.J. Fruehan, Thermodynamics of Ti in Ag–Cu alloys, Metall. Trans. B 21 (1990) 349–355.
[41] G.P. Kelkar, K.E. Spear, A.H. Carim, Thermodynamic evaluation of reaction products and layering in brazed alumina joints, J. Mater. Res. 9 (1994) 2244–2250.
[42] Coralie Valette, Marie-Francoise Devismes, Rayisa Voytovych, Nicolas Eustathopoulos, Interfacial reactions in alumina/CuAgTi braze/CuNi system, Scr. Mater. 52 (2005) 1–6.
[43] S. Suenaga, M. Nakahashi, M. Maruyama, T. Fukasawa, Interfacial reactions between sapphire and silver–copper–titanium thin film filler metal, J. Am. Ceram. Soc. 80 (1997) 439–444.
[44] F. Barbier, C. Peytour, A. Revcolevschi, Microstructural study of the brazed joint between alumina and Ti–6Al–4 V alloy, J. Am. Ceram. Soc. 73 (1990) 1582–1586.
[45] M. Paulasto, J. Kivilahti, Metallurgical reactions controlling the brazing of Al_2O_3 with Ag–Cu–Ti filler alloys, J. Mater. Res. 13 (1998) 343–352.
[46] R. Standing, M. Nicholas, The wetting of alumina and vitreous carbon by copper–tin–titanium alloys, J. Mater. Sci. 13 (1978) 1509–1514.
[47] E.K. Storms, Refractory Curbides, Academic Press, New York, 1967.
[48] H.-P. Xiong, W. Mao, Y.-H. Xie, W.-L. Guo, X.-H. Li, Y.-Y. Cheng, Brazing of SiC to a wrought nickel-based superalloy using CoFeNi(Si, B)CrTi filler metal, Mater. Lett. 61 (2007) 4662–4665.